RSC Advances

This is an *Accepted Manuscript*, which has been through the Royal Society of Chemistry peer review process and has been accepted for publication.

Accepted Manuscripts are published online shortly after acceptance, before technical editing, formatting and proof reading. Using this free service, authors can make their results available to the community, in citable form, before we publish the edited article. This *Accepted Manuscript* will be replaced by the edited, formatted and paginated article as soon as this is available.

You can find more information about *Accepted Manuscripts* in the Information for Authors.

Please note that technical editing may introduce minor changes to the text and/or graphics, which may alter content. The journal's standard Terms & Conditions and the Ethical guidelines still apply. In no event shall the Royal Society of Chemistry be held responsible for any errors or omissions in this *Accepted Manuscript* or any consequences arising from the use of any information it contains.

ROYAL SOCIETY OF CHEMISTRY

www.rsc.org/advances

Cite this: DOI: 10.1039/c0xx00000x

www.rsc.org/xxxxxx

ARTICLE TYPE

Photocatalytic and photoelectrochemical studies of Visible-light active α-Fe_2O_3-g-C_3N_4 nanocomposites

J. Theerthagiri [a], R.A. Senthil [a], A. Priya [a], J. Madhavan [a,*], R.J.V. Michael [b], Muthupandian Ashokkumar [c]

Received (in XXX, XXX) Xth XXXXXXXXX 20XX, Accepted Xth XXXXXXXXX 20XX
DOI: 10.1039/b000000x

Nanocrystalline hematite iron oxide (α-Fe_2O_3) and graphitic carbon nitride (g-C_3N_4) were prepared and used as precursors to synthesise α-Fe_2O_3-g-C_3N_4 composite photocatalysts of various compositions by wet impregnation method. The synthesized photocatalysts were characterized by x-ray diffraction (XRD), Fourier transform infrared spectroscopy (FT-IR), scanning electron microscopy (SEM), UV-vis diffuse reflection spectroscopy (DRS) and photoluminescence spectroscopy (PL). The efficiency of the photocatalysts was evaluated by photoelectrochemical measurements and photodegradation of direct red 81 (DR81) as a target textile pollutant under visible light irradiation. The α-Fe_2O_3-g-C_3N_4 composites exhibited remarkably improved visible-light induced photocatalytic activity. The composite photocatalysts with optimal α-Fe_2O_3 content with the highest photocatalytic activity was found to be 2%-α-Fe_2O_3-g-C_3N_4. The synergistic enhancement in the photocatalytic degradation of composite photocatalysts might be due to an increase in the visible-light absorption efficiency and rapid photoinduced charge separation. A possible photocatalytic mechanism has been proposed for the photocatalytic activity of α-Fe_2O_3-g-C_3N_4 composite photocatalysts.

1. Introduction

Semiconductor photocatalysis has received considerable attention in the areas of environmental remediation and energy storage, as it uses abundantly available solar energy.[1] The essential requirements of a photocatalyst is that it should be stable, inexpensive and capable of harvesting light in the visible region.[2] The main factor that lowers the efficiency of a photocatalsyt is the recombination rate of photo-generated electron-hole pairs.[3,4] Therefore, enormous effort has been made on the development of an efficient catalytic material for harvesting solar energy for photocatalytic degradation. Over the past few decades, various semiconductor materials such as metal oxides,[5,6] sulphides[7,8] and oxynitrides [9] have been identified as efficient photocatalysts for the degradation of toxic pollutants in water. Among the semiconductor materials, TiO_2 is the most widely used one because of its excellent catalytic activity, non-toxicity and stability. However, what greatly limits its practical application is its poor absorption in the visible region of the solar spectrum.[10]

More recently, graphitic carbon nitride (g-C_3N_4) material has been widely used as a metal-free visible light active photocatalyst. g-C_3N_4 has been extensively explored for the photocatalytic evolution of H_2 and O_2,[11] photodegradation of organic pollutants,[12] biomedical applications [13] and photocatalytic organic synthesis.[14] Nevertheless, a relatively low photocatalytic efficiency of pure g-C_3N_4 still limits its practical application due to the high recombination rate of photo-generated electron-hole pairs.[1] To resolve this problem and improve its photocatalytic performance, several methods have been developed, viz., doping of metals,[15] combining with other semiconductor material to form a composite photocatalytst [16] and sensitizing with organic dyes.[17] The combination of two semiconductors with different energy level may form an ideal system to cause a rapid charge separation and reduced recombination rate of photoinduced electron-hole pairs.[18] Very recently, remarkable progress has been made in the synthesis of composite photocatalysts. For example, g-C_3N_4-Fe_3O_4,[2] SiO_2/carbon nitride,[3] Ag_2O–g-C_3N_4,[15] Ni(OH)$_2$–g C_3N_4,[19] g–C_3N_4/$BiVO_4$,[20] Co_3O_4-g-C_3N_4 [21] and PANI-g-C_3N_4 [22] have been shown to exhibit high visible light photocatalytic activities than pure g-C_3N_4.

Ye et al.[23] synthesised Fe_2O_3/g-C_3N_4 from the precursor, melamine. In the present investigation, we have synthesised α-Fe_2O_3-g-C_3N_4 nanocomposite photocatalyst by a simple and low-cost method. Urea was chosen as a precursor for the synthesis of g-C_3N_4 because it is a low-cost raw material. α-Fe_2O_3 was synthesized using citrate route. α-Fe_2O_3 is an emerging material due to its superior properties such as high electrical conductivity and magnetic activity. α-Fe_2O_3 has high absoprtion (around 43%) in the red region of visible light in solar spectrum.[25] These properties of α-Fe_2O_3 makes it as a good candidate for coupling with g-C_3N_4 and improving its catalytic activities for the photodegradation of aqueous organic pollutants. Direct red 81 (DR81) was chosen for this study due to its harmful nature. DR81 is commonly used in the textile, leather, plastics and cosmetics industries to colour their products. These industries produce large volume of colored dye effluents which are toxic, non-biodegradable and cause a significant damage to the environment.

RSC Advances Accepted Manuscript

A series of α-Fe_2O_3-g-C_3N_4 composites with different mole percent of α-Fe_2O_3 were successfully synthesized and their visible light photocatalytic performances were evaluated for the photodegradation of DR81. A possible photocatalytic degradation mechanism has been proposed.

2. Experimental section

2.1 Materials

Urea, sodium sulphate and methanol were purchased from SDFCL India. Ferric nitrate nanohydrate was purchased from Qualigens India. Citric acid was obtained from Rankem India. Direct red 81 and demineralised water used in the experiments was purchased from Sigma-Aldrich and nice chemicals India, respectively. All reagents were of analytical grade and used without further purification.

2.2 Synthesis of photocatalysts

Ferric nitrate nanohydrate and citric acid (1:3 mole ratio) was dissolved in deionised water. The resulting solution was continuously stirred and subsequently dried at 95 ^{0}C. The obtained precipitate was heated in air atmosphere at 450 ^{0}C for 2 hours to produce α-Fe_2O_3 particles. g-C_3N_4 powders were synthesized by urea loaded in an alumina crucible with a cover to prevent sublimation of precursors and heated to 520 ^{0}C for 2 hours at a heating ramp of 15 ^{0}C/min and the furnace was cooled to room temperature naturally. The yellow colour product was collected and ground into a powder.

α-Fe_2O_3-g-C_3N_4 nanocomposite photocatalysts were prepared as follows: 0.5 g of g-C_3N_4 and calculated amount of as-prepared α-Fe_2O_3 were added into 40 mL of methanol in a beaker. Then the beaker was placed in an ultrasonic bath for 15 min. The mixed solution was magnetically stirred at 80 ^{0}C. The obtained product after volatilization of the methanol was sintered at 300 ^{0}C for 30 min. α-Fe_2O_3-g-C_3N_4 composite with different mole ratios 1%, 2% and 3% of α-Fe_2O_3 were prepared and are denoted in this manuscript as FOCN-1, FOCN-2 and FOCN-3, respectively.

2.3 Characterization of photocatalysts

The synthesized photocatalysts were characterized by powder x-ray diffraction (XRD) method using a powder x-ray diffractometer (Mini Flex II, Japan) with Cu Kα radiation (λ= 0.154 nm) at a scan speed of 3^0/min. The phase purity was ascertained using x-ray diffraction. The crystalline size was analyzed using Scherrer's equation, d=0.9λ/B cosθ, where d is the crystallite size, λ is the wavelength of x-ray radiation, B is the full width half maximum value (FWHM) in radian and θ is the diffraction angle. The micro-strain (ε) of the photocatalysts were estimated using the ε = B/4 tanθ equation. Fourier transform infrared (FT-IR) spectra were recorded (KBr pellets) with a wavenumber ranging from 4000-400 cm^{-1} using an FT-IR (JASCO 460 plus) instrument. The morphology of the products was examined by scanning electron microscopy (SEM) VEGA3TESCAN model. UV-vis diffuse reflectance spectra of the samples were recorded using a Shimadzu 2100 UV-vis spectrophotometer in the range of 200-800 nm. $BaSO_4$ was used as the reference. Photoluminescence (PL) measurements were recorded at room temperature using Jobin Yvon Flurolog-3-11 spectroflurometer. Radiation source was 450 W xenon lamp.

2.4 Photocatalytic activity

The photocatalytic activity of synthesized α-Fe_2O_3-g-C_3N_4 nanocomposites were studied by the photodegradation of direct red 81 (DR81) under visible light irradiation generated by a 100 W tungsten-halogen lamp. In each experiment, calculated amount of photocatalyst was mixed with 75 mL of $5x10^{-5}$ M solution of DR81. Prior to irradiation, the suspensions were magnetically stirred in the dark for 120 min to obtain the equilibrium adsorption of DR81 onto the catalyst. During irradiation 4 mL of aliquots were collected at fixed time intervals and filtered through a 0.45 µm membrane syringe filter (Pall Corporation) to remove the photocatalyst particles. The concentration of DR81 was monitored using a UV-vis spectrophotometer at 509 nm.

2.5 Photoelectrochemical studies

Photoelectrochemical measurements were performed on a CHI608E electrochemical workstation in a conventional three electrode configuration with a Pt-wire as counter electrode and Ag/AgCl (in saturated KCl) as a reference electrode. A 250 W Xe arc lamp (OSRAM, Germany) was used as the light source. A 0.1 M Na_2SO_4 aqueous solution was used as the electrolyte. The working electrode was prepared as follows: the 50 mg of photocatalyst was ground with 150 µL of PEG (Mol.Wt 400) and 125 µL of ethanol to make slurry. The slurry was spread on a 2.5x2.5 cm^2 fluorine-doped tin oxide (FTO) glass substrate with an active area of about 1x1 cm^2 by doctor-blade method using scotch tape as spacer. It was dried in air and then annealed at 350 ^{0}C for 45 min.

3. Results and Discussion

3.1 X-ray diffraction studies

The X-ray diffraction (XRD) patterns of α-Fe_2O_3, g-C_3N_4 and α-Fe_2O_3-g-C_3N_4 nanocomposites are shown in Fig. 1. The diffraction peaks of iron oxide synthesized from citrate precursor route at 2θ = 24.1^0, 33.1^0, 36.0^0, 40.8^0, 49.4^0 and 54.0^0 are in good agreement with the corresponding (012), (104), (110), (113) (024) and (116) diffraction planes of α-Fe_2O_3 (JCPDS 80-2377).[26] g-C_3N_4 shows two distinct diffraction peaks observed at 2θ = 13.06^0 and 27.42^0 which are indexed as (100) and (002) diffraction planes of graphitic carbon nitride material (JCPDS 87-1526). These diffraction peaks are in good agreement with earlier report by Ge et al.[22] The high intensity peak at 27.8^0 is a characteristic inter layer stacking peak of aromatic systems and the weak peak at 13.2^0 corresponds to the inter-layer structural packing of the tri-s-triazine pores.[27] The XRD patterns of as-synthesized α-Fe_2O_3-g-C_3N_4 composite photocatalysts consists of both α-Fe_2O_3 and g-C_3N_4 phases, the peak intensities in the composite sample is increased with mass content of α-Fe_2O_3 and

RSC Advances Accepted Manuscript

This journal is © The Royal Society of Chemistry [year]

it confirms the formation of α-Fe_2O_3-g-C_3N_4 composite material.[20, 28] The calculated crystalline size and micro-strain of the pure α-Fe_2O_3, g-C_3N_4 and α-Fe_2O_3-g-C_3N_4 nanocomposite materials are summarized in Table 1. It can be seen that the average crystalline size of the synthesised α-Fe_2O_3-g-C_3N_4 is around 4 to 5 nm and when compare with other composite materials, it is clear that the FOCN-2 showed the lower micro-strain value. The low micro-strain of FOCN-2 indicates the well crystalline nature of FOCN-2 composites.

Table 1 Crystalline size and micro-strain of the as-synthesized photocatalysts.

Sample	FWHM	Crystalline size (nm)	Micro-strain
α-Fe_2O_3	0.276	30.02	0.001089
g-C_3N_4	1.902	4.29	0.004418
FOCN-1	1.853	4.41	0.003761
FOCN-2	1.467	5.56	0.002839
FOCN-3	1.408	5.80	0.003178

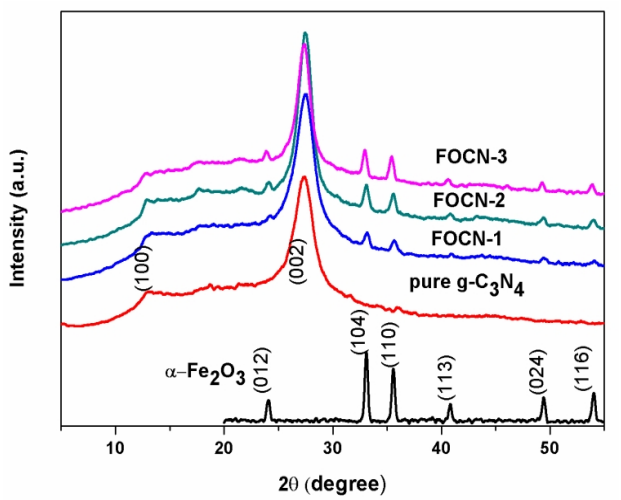

Fig. 1 XRD patterns of α-Fe_2O_3, g-C_3N_4 and α-Fe_2O_3-g-C_3N_4 photocatalysts.

3.2 FT-IR studies

Fourier transform infrared (FT-IR) spectra of α-Fe_2O_3, g-C_3N_4 and α-Fe_2O_3-g-C_3N_4 nanocomposites are shown in Fig. 2. In the FT-IR spectrum of α-Fe_2O_3, absorption bands at 473 cm^{-1} and 544 cm^{-1} are assigned to Fe-O stretching and bending vibration modes, respectively.[29] In the spectrum of g-C_3N_4, the broad band at 3100-3300 cm^{-1} can be assigned to the stretching modes of N-H bonds of primary (-NH_2) and secondary (=N-H) amines suggesting the hydrogenation of some nitrogen atoms in the g-C_3N_4.[30] The strong bands at 1200-1680 cm^{-1} are attributed to the stretching vibration modes of C-N heterocycles. The peaks at 1638 cm^{-1} and 1235 cm^{-1} are attributed to the stretching vibration modes of C=N and C-N, respectively.[31] The absorption peaks at 812 cm^{-1} corresponds to the characteristic ring breath of the triazine units. Further, the characteristic peaks of both α-Fe_2O_3 and g-C_3N_4 are appeared in the α-Fe_2O_3-g-C_3N_4 composite.

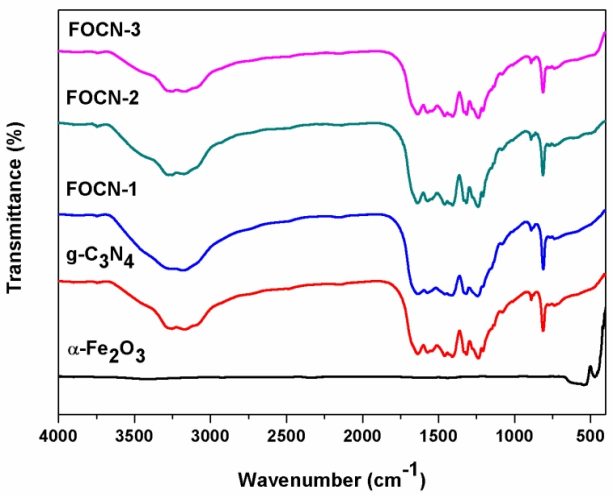

Fig. 2 FT-IR transmittance spectra of α-Fe_2O_3, g-C_3N_4 and α-Fe_2O_3-g-C_3N_4 photocatalysts.

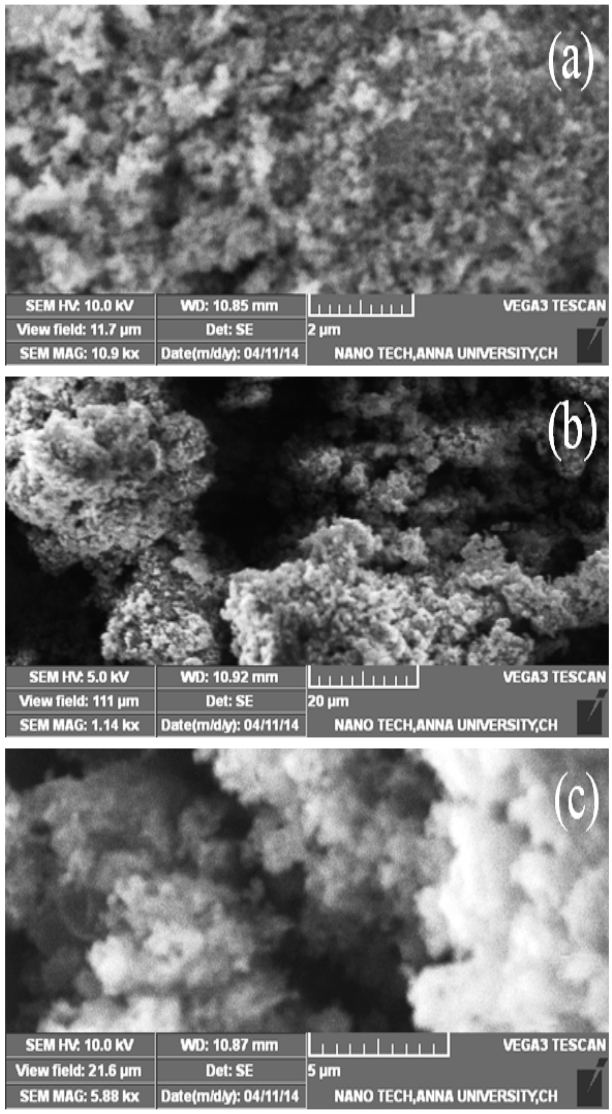

Fig. 3 Typical SEM photographs of (a) α-Fe_2O_3, (b) g-C_3N_4 and (c) FOCN-2.

RSC Advances Accepted Manuscript

The absorption peak intensity of g-C_3N_4 is decreased slightly while increasing the mole percent of α-Fe_2O_3 in the composite photocatalyst. The FT-IR results clearly indicate the coexistence of the α-Fe_2O_3 and g-C_3N_4 in the composite photocatalysts.

3.3 SEM and TEM studies

The typical SEM photographs of α-Fe_2O_3, g-C_3N_4 and FOCN-2 photocatalysts are presented in Fig. 3(a), (b) and (C), respectively. The SEM micrograph of α-Fe_2O_3 particles shows an aggregation of nanoparticles. The g-C_3N_4 shows the aggregated particles containing a large number of irregular smaller crystals. The morphology of FOCN-2 composites clearly shows that the narrower particle distribution on the porous structure of g-C_3N_4. The observed larger SEM particle sizes may be attributed to the larger cluster size which formed due to larger surface area of the smaller crystallites. A surface morphology where the composite particles are tightly packed is a benefit for the efficient charge carrier formation.[20] Further, the morphology and particle size of FOCN-2 were explored by TEM and the corresponding images are shown in Fig. 3(d) and (e). TEM images show fine dispersion of α-Fe_2O_3 on the surface of the g-C_3N_4 and the particle size of the α-Fe_2O_3 is found to be about 20 nm. Also, the TEM images of composite particles show some agglomeration.

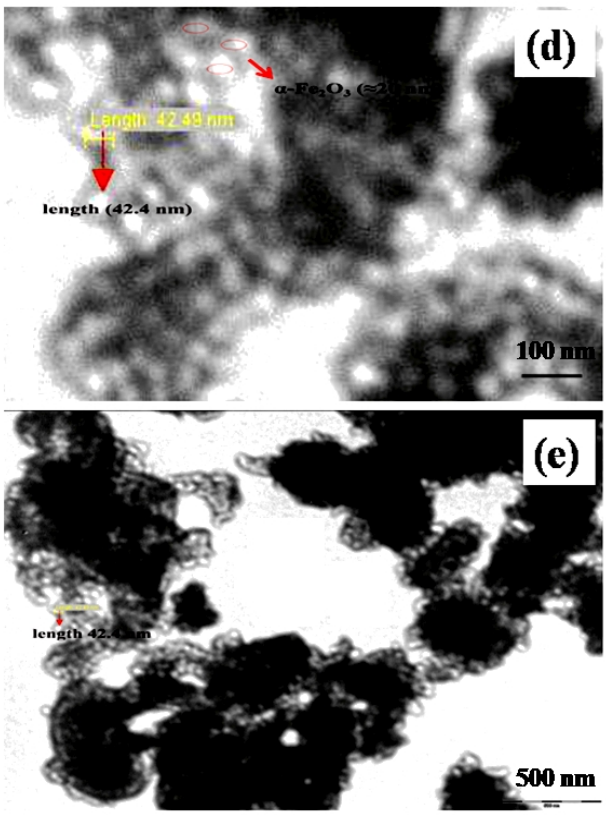

Fig. 3(d-e) TEM images of FOCN-2 photocatalyst particles.

3.4 Optical absorption studies

The optical properties of α-Fe_2O_3, g-C_3N_4 and α-Fe_2O_3-g-C_3N_4 nanocomposite were investigated by UV-vis diffuse reflectance spectroscopy and are shown in Fig. 4. g-C_3N_4 sample shows an absorption edge at 461 nm that corresponds to a band gab energy of 2.68 eV. This is in good agreement with the band gap energy reported in the literature.[23] Hence, it can act as a good photocatalyst under visible light irradiation. The absorption edge value for α-Fe_2O_3 is observed at 686 nm and the corresponding band gab is estimated to be about 1.80 eV. The absorption edges of α-Fe_2O_3-g-C_3N_4 nanocomposites samples are significantly increased with an increase in the content of α-Fe_2O_3. That is a red shift in the absorption edge on increasing the α-Fe_2O_3 loading and also the powder colour changed from yellowish to light grey. This result implies that the charge-transfer transition between the α-Fe_2O_3 and g-C_3N_4 species occurs while adding α-Fe_2O_3 to g-C_3N_4. This subsequently indicate that the composite samples could absorb a major portion of light in the visible region to produce electron-hole pairs and that may in-turn lead to high photocatalytic activity of the composite catalysts.

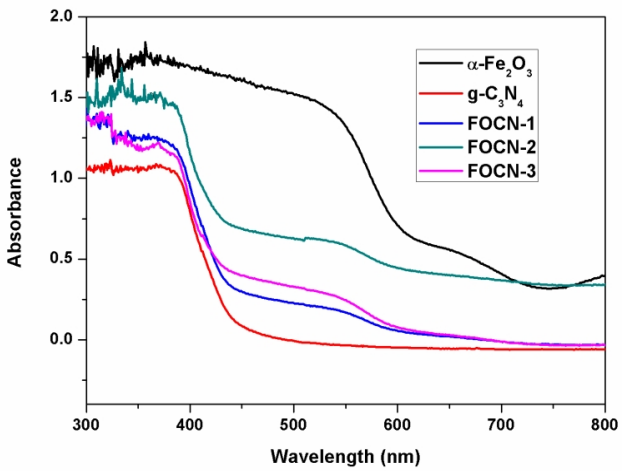

Fig. 4 UV-vis diffuse reflection spectra of α-Fe_2O_3, g-C_3N_4 and α-Fe_2O_3-g-C_3N_4 photocatalysts.

3.5 Photocatalytic performance of the α-Fe_2O_3-g-C_3N_4 nanocomposites

The photocatalytic efficiencies of α-Fe_2O_3-g-C_3N_4 nanocomposites were evaluated using DR81 as a model pollutant under visible irradiation. A blank experiment in the absence of catalyst was carried out for the dye alone ($5x10^{-5}$ M) under visible light irradiation for 2 hours. There was no significant change in absorbance of DR81 indicating the stable nature of the dye under visible light irradiation. Also, adsorption efficiency of DR81 on the photocatalyst was evaluated in the dark to identify the time taken to reach the adsorption-desorption equilibrium. It was found that the equilibrium between the catalyst and dye was established after 90 min of stirring (results not shown). The photocatalytic activities of g-C_3N_4, α-Fe_2O_3 and α-Fe_2O_3-g-C_3N_4 nanocomposites with different loading amount (1%, 2% and 3% mole content) of α-Fe_2O_3 are shown in Fig. 5(a). No significant

RSC Advances Accepted Manuscript

This journal is © The Royal Society of Chemistry [year]

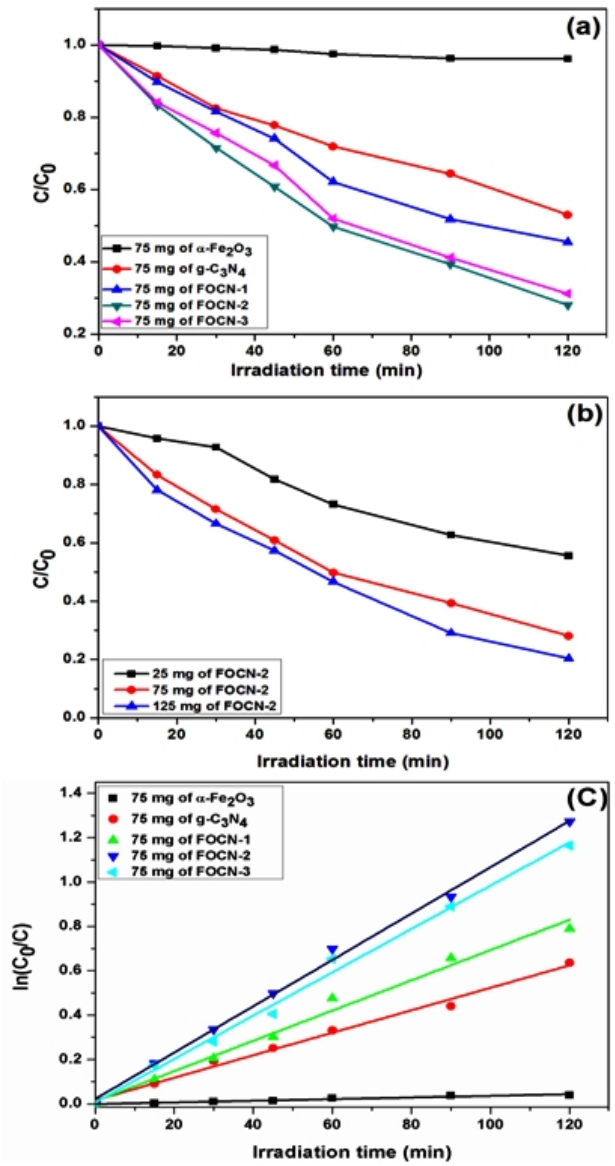

Fig. 5 (a) Photocatalytic degradation of DR81 over α-Fe_2O_3, g-C_3N_4 and α-Fe_2O_3-g-C_3N_4 photocatalysts under visible light irradiation, (b) Photocatalytic degradation of DR81 over FOCN-2 photocatalyst at different amounts; 0.5 g/L, 1.0 g/L and 1.25 g/L, (c) First-order kinetics plot for the photodegradation of DR81 over α-Fe_2O_3, g-C_3N_4 and α-Fe_2O_3-g-C_3N_4 photocatalysts.

degradation was observed with α-Fe_2O_3 alone. Pradhan et al.[25] reported that though α-Fe_2O_3 has high absorption in the red region of visible spectrum (around 43 %), its efficiency for the photocatalytic performance is limited due to the charge carrier recombination. However, a significant decrease in the absorbance of the dye is observed when g-C_3N_4 is used as a photocatalyst. This is due to the involvement of photo-generated produced electron and hole pairs in the degradation process. It can be seen that α-Fe_2O_3-g-C_3N_4 composites exhibit much higher photodegradation activities than that of g-C_3N_4 and the photocatalytic activity increases remarkably up to 2% increase the amount of α-Fe_2O_3. It is noted that there exists a synergy in the degradation rate when the composite material is used. This might be due to the higher absorption of light in the visible region. It can be noted that the photodegradation rate attained saturation on further increasing the content of α-Fe_2O_3. The optimum photocatalytic activity of α-Fe_2O_3-g-C_3N_4 is found to be at 2% α-Fe_2O_3 loading and therefore under the experimental conditions used.

The effect of catalyst amount on the photocatalytic degradation of DR81 was performed with the best composite by keeping other experimental parameters constant. Fig. 5(b) shows the photocatalytic activity of best performing sample FOCN-2 with different catalyst amounts of 0.5 g/L, 1.0 g/L and 1.25 g/L. It is seen from Fig. 5(b) that the photocatalytic degradation rate increases with an increase in catalyst loading and this may be due to increase in the number of available catalyst sites for light absorption which generates more electron-hole pairs for dye degradation and consequently enhances the degradation rate.

The experimental data were fitted by a first-order kinetic equation (1) to investigate the reaction kinetics of the DR81 photodegradation by α-Fe_2O_3, g-C_3N_4 and various α-Fe_2O_3-g-C_3N_4 composite photocatalysts.

$$\ln C_o/C = kt \qquad \text{------} \qquad (1)$$

where k is the first-order rate constant (min^{-1}), t is the irradiation time (min), C_o and C is the initial concentration and concentration of DR81 at regular time intervals. It can be seen from the data shown in Figure 5(c) that the degradation process followed first order kinetics.

3.6 Photoluminescence studies

Photoluminescence (PL) spectral analysis is used to investigate the recombination processes of photoinduced electron-hole pairs in the composite materials. The PL spectra of α-Fe_2O_3, g-C_3N_4 and α-Fe_2O_3-g-C_3N_4 composite photocatalysts are shown in Fig. 6. The excitation wavelength for α-Fe_2O_3 was at 265 nm and 325 nm was used for g-C_3N_4 and α-Fe_2O_3-g-C_3N_4. The main emission band is centred at about 462 nm for g-C_3N_4 and the peak position of composite photocatalysts in the PL spectra are similar to that of g-C_3N_4 but the intensity of emission peaks is significantly decreased. This indicates that the recombination rate of photogenerated electron-hole pairs is very low for the composite photocatalysts .[2,22] It can be observed that there is no clear correlation between in the PL intensity and the incremental addition of α-Fe_2O_3 to g-C_3N_4. PL intensity trend is in the order, FOCN1>FOCN3>FOCN2. The observed PL trend supports the trend observed for the photocatalytic degradation efficiency. That is, FOCN-2 catalyst showed the weakest intensity, which supports the photocatalytic degradation results discussed in the previous section. Therefore, the FOCN-2 composite is the best composition for the photocatalytic degradation of DR81. However, the actual reason for the observed PL trend needs further investigation.

RSC Advances Accepted Manuscript

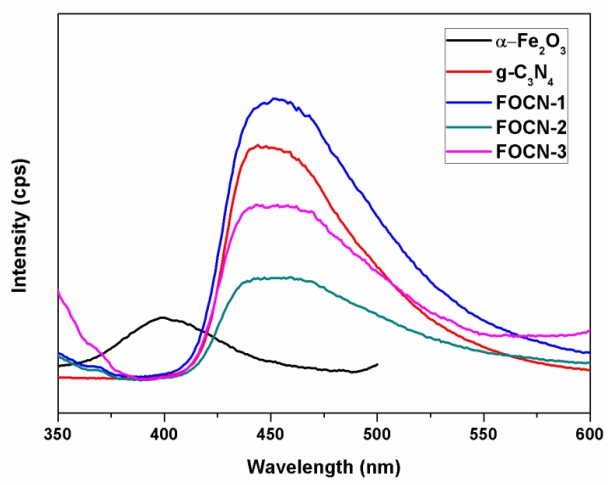

Fig. 6 Photoluminescence spectra of the as-synthesized pure α-Fe_2O_3, g-C_3N_4 and α-Fe_2O_3-g-C_3N_4 photocatalysts.

3.7 Photoelectrochemical studies

Photoelectrochemical study was carried out to give further support of the proposed photocatalytic activity of FOCN-2. The transient-photocurrent response of g-C_3N_4 and FOCN-2 were recorded for light on-off cycles under visible light irradiation and the results are shown in Fig. 7(a). It is clear that FOCN-2 generates higher photocurrent than that of g-C_3N_4. The photocurrent enhancement of FOCN-2 indicated an enhanced charge carrier (electron and hole) separation. The observed high photocatalytic degradation in the presence of FOCN-2 may be attributed to the reduced recombination rate of charge carriers as supported from the transient photocurrent studies.

The reaction rate occurring on the surface of the electrode is reflected by the arc radius of the Nyquist impedance plots.[32] Electrochemical impedance study was performed for g-C_3N_4 and FOCN-2 samples to know the interfacial electron transfer rate. The corresponding Nyquist plots with and without light illumination are shown in Fig. 7(b). It is found that the arc radius of FOCN-2 is smaller than that of g-C_3N_4 indicating a more effective separation efficiency of photogenerated electron-hole pairs and a faster interfacial charge transfer. This shows a more favourable condition for enhanced photocatalytic activity of FOCN-2 composite.

3.8 Photocatalytic mechanism

A possible mechanism has been proposed for the synergistic effect of α-Fe_2O_3-g-C_3N_4 photocatalyst for the photocatalytic degradation of DR81 and a schematic diagram representing the series of possible photochemical events is illustrated in Fig. 8. Photocatalytic activity of α-Fe_2O_3-g-C_3N_4 composite is much higher than that of g-C_3N_4. The conduction band (CB) of g-C_3N_4 is -1.12 eV and the valance band is 1.57 eV.[1] Whereas by knowing the E_g, the conduction band (CB) and valence band (VB) potentials of α-Fe_2O_3 are calculated using the Equation (2)[33-35]

$$E_{VB} = X\text{-}E^e + 0.5E_g \quad \text{------} \quad (2)$$

where E_{VB} is the valence band edge potential, X is the electronegativity of the semiconductor, for α-Fe_2O_3 absolute electronegativity is 5.89, E^e is the energy of free electrons on the hydrogen scale (~4.5 eV).

The obtained E_{VB} value using the above equation is 0.49 eV and from the E_{VB} value, we can determine the E_{CB} value using Equation (3).

$$E_{CB} = E_{VB}\text{-}E_g \quad \text{------} \quad (3)$$

The calculated CB and VB edge potentials of α-Fe_2O_3 are 0.49 and 2.29 eV, respectively.

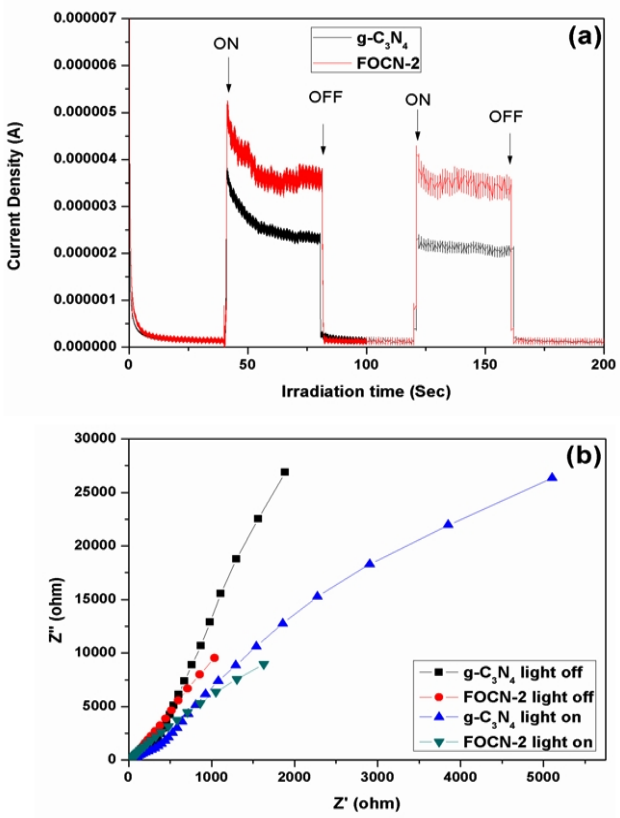

Fig. 7 (a) Transient-photocurrents of pure g-C_3N_4 and FOCN-2 under visible light irradiation, (b) Nyquist plot of g-C_3N_4 and FOCN-2 photocatalysts with and without visible light illumination.

The conduction band edge potential of g-C_3N_4 is more negative than that of α-Fe_2O_3. Thus the photoinduced electrons transfer from g-C_3N_4 into the CB of α-Fe_2O_3, while the holes are transferred to VB of g-C_3N_4. The recombination process of electron-hole pair is decreased and increases the charge separation, which leads to the more photocatalytic activity of α-Fe_2O_3-g-C_3N_4 composite.

RSC Advances Accepted Manuscript

This journal is © The Royal Society of Chemistry [year]

The possible photocatalytic reactions are similar to those reported in the literature[22,31] as follows:

$\alpha\text{-}Fe_2O_3\text{-}g\text{-}C_3N_4 + hv \longrightarrow \alpha\text{-}Fe_2O_3\ (e^-_{CB}) + g\text{-}C_3N_4\ (h^+)$

$\alpha\text{-}Fe_2O_3\ (e^-_{CB}) + O_2 \longrightarrow O_2^-$

$O_2^- + 2\ e^-_{CB} + 2H^+ \longrightarrow {}^{\cdot}OH + OH^-$

$g\text{-}C_3N_4\ (h^+) + H_2O \longrightarrow H^+ + {}^{\cdot}OH$

$DR81 + {}^{\cdot}OH \longrightarrow$ oxidation products (CO_2, H_2O etc)

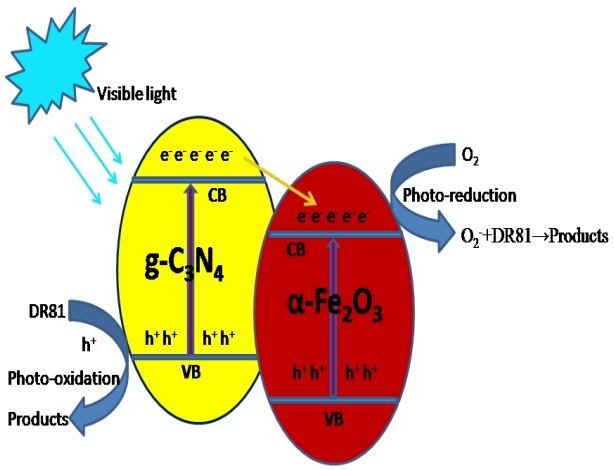

Fig. 8 Schematic illustration of the mechanism of electron-hole separation and photocatalytic degradation of DR81 over $\alpha\text{-}Fe_2O_3\text{-}g\text{-}C_3N_4$ photocatalyst under visible light irradiation.

4. Conclusion

In summary, nanocrystalline $\alpha\text{-}Fe_2O_3$ and $g\text{-}C_3N_4$ phases were synthesized by simple and cost effective processes. Using these as precursors, $\alpha\text{-}Fe_2O_3\text{-}g\text{-}C_3N_4$ nanocomposite photocatalysts with different amounts of $\alpha\text{-}Fe_2O_3$ were successfully synthesized by wet impregnation method. The interaction between the $\alpha\text{-}Fe_2O_3$ and $g\text{-}C_3N_4$ in the composite and phase formation was confirmed by the FT-IR and XRD studies. The addition of $\alpha\text{-}Fe_2O_3$ significantly affected the optical properties of the photocatalysts. The $\alpha\text{-}Fe_2O_3\text{-}g\text{-}C_3N_4$ composites exhibited the highest photocatalytic activity than $\alpha\text{-}Fe_2O_3$ and $g\text{-}C_3N_4$ for the degradation of DR81 under visible light irradiation. The composite photocatalyst with 2 mol% of $\alpha\text{-}Fe_2O_3$ was found to show the highest photocatalytic activity. The photoelectrochemical studies further confirmed the superior activity of the FOCN-2 photocatalyst. A possible photocatalytic mechanism has been proposed based on the photodegradation results. The reason for the high photocatalytic activity may be attributed by the increase of interfacial electron transfer process and decrease of the electron-hole recombination rate. The present investigation provides strong evidence that $\alpha\text{-}Fe_2O_3\text{-}g\text{-}C_3N_4$ nanocomposites are promising photocatalytic materials in efficient utilization of solar energy for the treatment of polluted wastewaters and also other environmental remediation processes.

Acknowledgements

We gratefully acknowledge the financial support from Department of Atomic Energy-Board of Research in Nuclear Sciences (DAE-BRNS), Mumbai and Department of Science and Technology (DST), New Delhi, India.

Notes and references

[a] *Solar Energy Lab, Department of Chemistry, Thiruvalluvar University, Vellore-632 115, India. Fax: +91 416 2274748; Tel: +91 416 2274747; E-mail: jagan.madhavan@gmail.com (J. Madhavan)*

[b] *Department of Chemistry, Anna University, Chennai-600 025, India.*

[c] *School of Chemistry, University of Melbourne, Parkville campus, Melbourne, VIC 3010, Australia.*

1 J.X. Sun, Y.P. Yuan, L.G. Qiu, X. Jiang, A.J. Xie, Y.H. Shen and J.F. Zhu, *Dalton Trans.*, 2011, **41**, 6756.

2 S. Kumar, T. Surendar, B. Kumar, A. Baruah and V. Shankar, *J. Phys. Chem., C* 2013, **117**, 26135.

3 M. Shaloma, S. Inalb, D. Neherb and M. Antonietti, *Catal. Today*, 2014, **225,** 185.

4 Y. Wang, R. shi, J. Lin and Y. Zhu, *Energy Environ. Sci.*, 2011, **4**, 2922.

5 Y.C. Chang, *RSC Adv.*, 2014, **4**, 20273.

6 M.H. Khedr, K.S. Halim, N.K. Soliman, *Mater. Lett.*, 2009, **63**, 598.

7 X.H. Guan, P. Qu, X. Guan and G.S. Wang, *RSC Adv.*, 2014, **4**, 15579.

8 K. Zhang and L. Guo, *Catal. Sci. Technol.*, 2013, **3,** 1672.

9 R. Nakamura, T. Tanaka and Y. Nakato, *J. Phys. Chem. B*, 2005, **109**, 8920.

10 U.G. Akpan and B.H. Hameed, *J. Hazard. Mater.*, 2009, **170**, 520.

11 G. Zhang, J. Zhang, M. Zhang and X. Wang, *J. Mater. Chem.*, 2012, **22**, 8083.

12 F. Dong, Y. Sun, L. Wu, M. Fu and Z. Wu, *Catal. Sci. Technol.*, 2012, **2**, 1332.

13 L.S. Lin, Z.X. Cong, J. Li, K.M. Ke, S.S. Guo, H.H. Yang and G.N. Chen, *J. Mater. Chem. B*, 2014, **2**, 1031.

14 H. Zhan, W. Liu, M. Fu, J. Cen, J. Lin, H. Cao, *Appl. Catal. A: General* 2013, **468**, 184.

15 X. Ma, Y. Lv, J. Xu, Y. Liu, R. Zhang and Y. Zhu, *J. Phys. Chem.* C, 2012, **116**, 23485.

16 L. Shi, L. Liang, J. Ma, F. Wang and J. Sun, *Catal. Sci. Technol.*, 2014, **4**, 758.

17 K. Takanabe, K. Kamata, X. Wang, M. Antonietti, J. Kubota and K. Domen, *Phys. Chem. Chem. Phys.*, 2010, **12**, 13020.

18 Y. Liu, L. Yu, Y. Hu, C. Guo, F. Zhanga and X. W. Lou, *Nanoscale*, 2012, **4**, 183.

19 J. Yu, S. Wang, B. Cheng, Z. Lin and F. Huang, *Catal. Sci. Technol.*, 2013, **3**, 1782.

20 Y. Ji, J. Cao, L. Jiang, Y. Zhang, Z. Yi, *J. Alloys Compd.*, 2014, **590**, 9.

21 C. Han, L. Ge, C. Chen, Y. Li, X. Xiao, Y. Zhang and L. Guo, *Appl. Catal. B: Environmental*, 2014, **147**, 546.

22 L. Ge, C. Han and J. Liu, *J. Mater. Chem.*, 2012, **22**, 11843.

23 S. Ye, L.G. Qiu, Y.P. Yuan, Y.J. Zhu, J. Xia and J.F. Zhu, *J. Mater. Chem. A*, 2013, **1**, 3008.

24 S. Podsiadlo, *Thermochim. Acta*, 1995, **256**, 375.

25 G.K. Pradhan, D.K. Padhi and K. M. Parida, *ACS Appl. Mater. Interfaces*, 2013, **5**, 9101.

26 P.P. Sarangi, S.R. Vadera, M.K. Patra, C. Prakash, and N.N. Ghosh, *J. Am. Ceram. Soc.*, 2009, **92**, 2425.

RSC Advances Accepted Manuscript

27 F. Chang, Y. Xie, C. Li, J. Chen, J. Luo, X. Hu, J. Shen, *Appl. Surf. Sci.*, 2013, **280**, 967.
28 Y. He, L. Zhang, X. Wang, Y. Wu, H. Lin, L. Zhao, W. Weng, H. Wan and M. Fan, *RSC Adv*., 2014, **4**, 13610.
29 B. Zhao, Y. Wang, H. Guo, J. Wang, Y. He, Z. Jiao, M. Wu, *Mater. Sci. Poland*, 2007, **25**, 1143.
30 F. Yang, V. Kuznietsov, M. Lublow, C. Merschjann, A. Steigert, J. Klaer, A. Thomas and T.S. Niedrig, *J. Mater. Chem. A.*, 2013, **1**, 6407.
31 H. Ji, F. Chang, X. Hu, W. Qin, and J. Shen, *Chem. Eng. J*., 2013, **218**, 183.
32 H. Xu, J. Yan, X. She, L. Xu, J. Xia, Y. Xu, Y. Song, L. Huang and H. Li, *Nanoscale*, 2014, **6**, 1406.
33 S. Bai, K. Zhang, J. Sun, R. Luo, D. Li, A. Chen, CrystEngComm, 2014, **16**, 3289–3295.
34 X. Lin, J. Xing, W. Wang, Z. Shan, F. Xu, F. Huang, J. Phys. Chem. C 2007, **111**, 18288-18293.
35 Y. Xu, M.A.A. Schoonen, Am. Mineral. 2000, **85**, 543-556.

RSC Advances Accepted Manuscript

This journal is © The Royal Society of Chemistry [year]

Photocatalytic and photoelectrochemical studies of Visible-light active α-Fe_2O_3-g-C_3N_4 nanocomposites

J. Theerthagiri, R.A. Senthil , A. Priya, J. Madhavan*, R.J.V. Michael, Muthupandian Ashokkumar

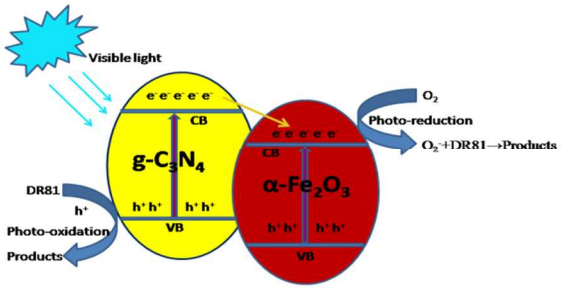

Synergistic enhancement in photocatalytic degradation of α-Fe_2O_3-g-C_3N_4 due to an increase in visible-light absorption efficiency and rapid photoinduced charge separation.

RSC Advances Accepted Manuscript